Inner-Paddled Atomic Force Microscopy Cantilever for Rapid Mechanical Mapping

Xu Yang,[1] Chengfu Ma,[2,*] Xiuxia Wang,[3] and Chenggang Zhou[3,*]

[1] *School of Microelectronics, University of Science and Technology of China, Hefei 230026, China*
[2] *CAS Key Laboratory of Mechanical Behavior and Design of Materials, Department of Precision Machinery and Precision Instrumentation, University of Science and Technology of China, Hefei 230026, China*
[3] *Center for Micro- and Nanoscale Research and Fabrication, Hefei National Research Center for Physical Sciences at the Microscale, University of Science and Technology of China, Hefei 230026, China*

(Dated: May 12, 2023)

Mechanical characterization methods at the nanoscale are of critical importance for many fields including nanomaterials, micro/nano devices and nanomechanics. As a key tool in nanotechnology, atomic force microscopy (AFM) is widely used due to its high-resolution topography imaging capabilities, and is also recognized as a useful platform for nanoscale mechanical characterization. Contact-resonance AFM, which modulates the tip-sample contact with ultrasonic frequencies and then analyzes the cantilever's resonance responses, is an important AFM method for viscoelastic characterization. However, contact-resonance AFM requires the cantilever's contact-resonance frequency and quality factor values to quantify the elastic modulus and loss tangent of the sample. This requires time-consuming frequency sweep, which makes a quantitative scanning impractical, therefore only single-point quantitative measurement and qualitative single-frequency scanning are usually applied. To address this issue, here we present an AFM cantilever design with an integrated inner-paddle substructure, which provides an eigenmode whose resonance keeps consistent, but whose resonance amplitude varies with varying contact stiffness. With this probe, it is hoped to quantify the elastic properties of the sample with fast single-frequency amplitude imaging.

Keywords: atomic force microscopy; contact resonance; cantilever design; mechanical characterization; contact stiffness

1. INTRODUCTION

Mechanical characterization techniques at the micro- and nanoscale are becoming increasingly important in the thriving fields of nanomaterials and micro/nano devices [1]. While mostly known as a high-resolution topographical imaging tool in nanotechnology, atomic force microscopy (AFM) [2] has also become as a promising platform for mechanical characterization at the nanoscale. Many different AFM-based nanomechanical measurement methods have been developed which show promising applications [3]. Among the most used ones are the quasi-static force-distance curve method and its derivatives [4, 5], the intermittent-contact multifrequency methods [6], and the contact-resonance technique [7, 8]. While the force-distance curve and multifrequency AFM methods are mostly applicable for soft materials [3], contact-resonance AFM is applicable for viscoelastic properties measurements of samples in a broad modulus range from soft polymers [8] to stiff materials with elastic moduli of $\sim$ 100 GPa [7]. Meanwhile, contact-resonance AFM also attracts intense attentions due to its capability of noninvasive imaging of mechanically heterogeneous subsurface structures [9].

Contact-resonance AFM characterizes the mechanical properties of a sample by measuring the changes of the cantilever's resonances induced by the tip-sample contact [7, 8]. To do so, the sample or the cantilever is acoustically excited by respectively a transducer installed beneath the sample or by the piezo shaker in the cantilever holder while the AFM is scanning the sample in the contact mode [9]. The frequencies and quality factors of the cantilever's contact resonances are then measured, from which the contact stiffness and damping between the tip-sample contact is characterized by adopting appropriate resonance model for the cantilever beam [7, 8]. Finally, the elastic modulus [7] and the loss tangent [8] of the sample are deduced by considering suitable contact mechanics models.

Quantitative mechanical characterization by contact-resonance AFM requires recording the contact-resonance spectrum. However, a spectroscopy measurement by frequency sweep is quite time-consuming, and a quantitative point-by-point contact-resonance AFM mapping with an acceptable resolution, for instance 256×256 pixels, usually takes almost an hour to finish. Due to this shortcoming, quantitative contact-resonance spectroscopy measurements are performed only at fixed points of interests on the sample surface. To have an overall understanding of the mechanical distribution of the sample surface, qualitative contact-resonance AFM imaging is usually carried out. In such a method, the amplitude and phase signals at a fixed working frequency that is near the contact resonance are mapped instead of the frequency and quality factor parameters [9]. However, the resulting amplitude and phase images can not be used

* Corresponding authors: chfuma@ustc.edu.cn (C. M.); cgzhou@ustc.edu.cn (C. Z.)

to infer the mechanical properties of the sample surface, whose contrasts depends on the working frequency. In fact, even contrast reversals can be observed by using different working frequencies [10]. To overcome the problem of time-consuming spectroscopy measurement, novel resonance analyzing methods have been proposed, including a dual-frequency resonance-tracking technique [11] and a band excitation method [12]. However, both methods require costly excitation and tracking hardware. In addition, in the dual-frequency resonance-tracking technique, tracking error is unavoidable since it assumes a damped harmonic oscillator model for the resonances which deviates from real measurements [13].

Here, in this article, we propose an inner-paddled AFM cantilever design as an alternative to address the problem of time-consuming spectroscopy measurement in contact-resonance AFM. The proposed cantilever contains a secondary small cantilever that is integrated inside a normal rectangular cantilever. Such a cantilever provides a resonance mode whose frequency keeps relatively stable within a broad range of contact stiffness, whereas its amplitude corresponds monotonically to the changes of the tip-sample contact stiffness. Therefore, by simply measuring the amplitude changes during scanning, a semi-quantitative stiffness mapping of the sample can be obtained. This avoids the time-consuming resonance frequency measurement by frequency sweep, and also addresses the issue of contrast reversals in qualitative contact-resonance AFM imaging.

It should be mentioned that similar cantilever designs have been previously employed for signal enhancement in multi-harmonic AFM [14] and for topographic effect decoupling in piezoresponse force microscopy (PFM) [15]. Especially, Dharmasena *et al* [15] have introduced an inner-paddled AFM cantilever design which provides a stable contact resonance that is independent of the local contact stiffness changes. Such a cantilever has been demonstrated to be beneficial for addressing the coupling effect of surface topography, which induces local contact stiffness changes, in characterizing the functional responses of piezoelectric and ferroelectric materials with PFM [15]. Although based on a similar conceptual design as that of Dharmasena *et al* [15], our design differentiates from theirs by not varying the thickness of the inner-paddled cantilever, which facilitates the fabrication. More importantly, we demonstrate here the additional benefit of using such an inner-paddled cantilever for fast mechanical mapping of materials, by avoiding time-consuming frequency sweep measurement in contact-resonance AFM for quantitative mechanical characterization.

2. INNER-PADDLED CANTILEVER DESIGN AND FABRICATION

2.1. Inner-Paddled Cantilever Design.

As schematically shown in Fig. 1(a), a rectangular cantilever is usually used in contact-resonance AFM. The interaction due to the tip-sample contact changes the boundary condition of the cantilever beam, and thus shifts its vibration modes from the free resonances to higher contact resonances. The resonance shifts are determined by the contact stiffness exerted at the tip, which is defined by the tip shape, the contact force applied between the tip and sample, as well as by their elastic properties [7]. For example, under the same tip load, a stiffer sample with larger Young's modulus will shift the cantilever resonance to a higher frequency, as schematically illustrated in Fig. 1(b). By adopting an appropriate resonance model for the cantilever beam [7, 8], its resonance frequencies can be theoretically determined as a function of the contact stiffness as schematically shown in Fig. 1(c) by the dispersion curves representing respectively its first three flexural eigenmodes. From such dispersion curves, the contact stiffness is firstly deduced from the measured contact-resonance frequency and then the indentation modulus is estimated by adopting a suitable contact mechanics model [7].

Instead of informing the sample's stiffness through the cantilever's resonance shift which requires time-consuming spectroscopy measurement, here we propose a cantilever design which has an eigenmode whose frequency changes little but whose amplitude is sensitive to contact stiffness variations. The proposed cantilever contains a secondary small paddle-like cantilever integrated inside a hollow cantilever near its tip end, see the schematic shown in Fig. 1(d). As illustrated in Fig. 1(e), since the free end of the inner cantilever is not in direct contact with the sample, its resonance frequency will change little to the changes of the tip-sample contact stiffness. Meanwhile, due to smaller tip indentation, for a larger tip-sample contact stiffness case, excitations from the cantilever chip end or from the sample surface can be more effectively transferred to the inner cantilever, resulting in larger resonance amplitude. Compared to conventional cantilevers used in contact-resonance AFM, our proposed inner-paddled cantilever would have an eigenmode that doesn't change in a wide range of tip-sample contact stiffness, as schematically shown in Fig. 1(f).

2.2. Simulation and Fabrication.

Since a wide range of contact stiffness is usually encountered in real experiments, the proposed inner-paddled cantilever should be designed so that its new eigenmode induced by the secondary small cantilever keeps stable in such a contact stiffness range (Fig. 1(f)). To do so, we use finite element analysis (FEA) simula-

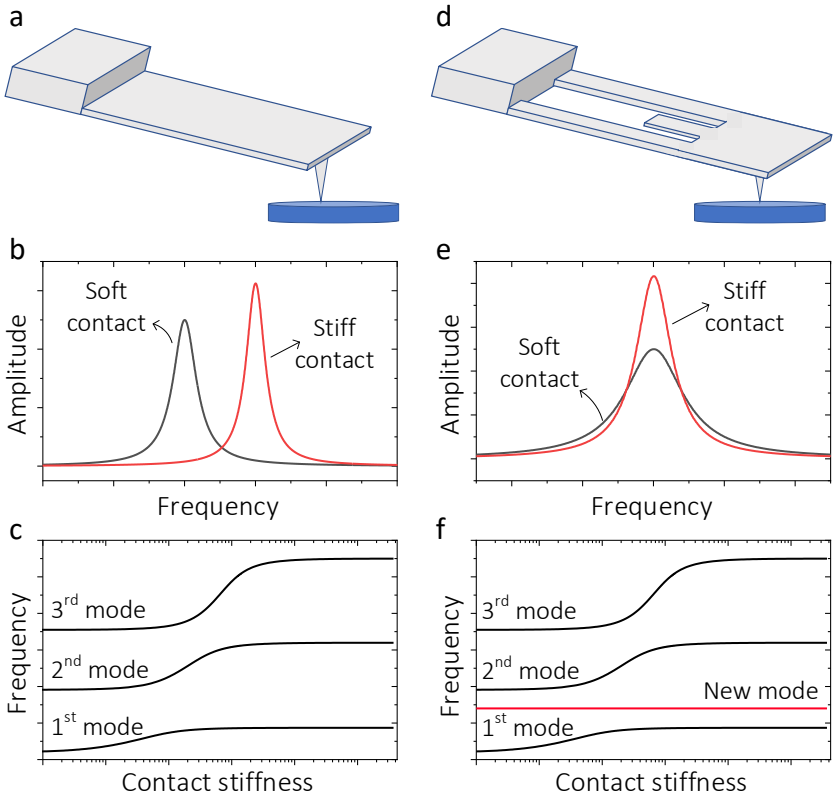

FIG. 1. (a) Schematic diagram of a rectangular cantilever conventionally used in contact-resonance AFM, with illustrations of (b) its resonances for respectively a soft and a stiff contact and (c) the frequencies of its first three flexural eigenmodes as functions of the applied contact stiffness. (d)(e)(f) are same as of (a)(b)(c) but for the inner-paddled cantilever design, for which a new eigenmode with stable resonance frequency in a large contact stiffness range is expected.

tions to design the cantilever structure. A schematic of the analysis model is shown in Fig. 2(a), where the cantilever is clamped at one end and its tip is coupled to the sample with the tip-sample interaction being modeled by elastic springs both in the normal and lateral directions with respective stiffnesses of k_N and k_L. The cantilever is set to have a fixed length of $L = 450$ μm, a width of $W = 50$ μm, and a thickness of $T = 2$ μm for the base cantilever. The tip height is set to be $H = 17$ μm with a center location of $L_t = 15$ μm from the cantilever's free end. In addition, a cantilever tilt of 11° relative to the surface plane is set here considering technical reason of cantilever mounting in AFM systems [7]. However, our additional simulation on a model without cantilever tilt shows that such a parameter has negligible effect on the resonance of the new eigenmode induce by the inner cantilever. The parameters defining the inner cantilever structures, including its position L_1 accounting from the cantilever's clamped end, its length L_2, its width W_2 are optimized to meet the design target. Although the thickness of the inner cantilever is another effective parameter for optimizing the design, it is set as same as the thickness of the base cantilever considering fabrication convenience. For example, Dharmasena *et al* has reported an inner-paddled cantilever design with an inner cantilever as thin as 300 nm integrated inside a normal commercial AFM cantilever with a thickness of approx. 1.6 μm [15]. However, it requires complicated processes to assemble the small cantilever to the base cantilever [15]. Direct fabrication of an inner cantilever by thinning with focused ion beam (FIB) based machining usually results in curling or destruction of the inner cantilever (data not shown). In addition, the hollow structure hosting the inner cantilever is set to end at the cantilever clamped end and has a width of $W_1 = W_2 + 4$ μm.

We then carry out modal analyses for the cantilever model in Fig. 2(a) by using the FEA software Comsol Multiphysics. The resonance frequencies of the cantilever's first several eigenmodes are calculated for various parameter sets for the inner cantilever structure (see above). For different parameter sets, calculations are done for a wide range of contact stiffness over k_N=10∼1000 N/m, which covers most experiments conditions. The lateral contact stiffness k_L is assumed to be 0.85 times of the normal one k_N, as it is for most materials [16]. Within the above contact stiffness range, changes of the frequencies of each mode are calculated and the structure parameters are optimized in a multi-parameter space to meet the target that one of the eigenmode has a frequency change smaller than 2 kHz. For this target, a set of suitable inner-paddled cantilever designs can be obtained. For example, in Fig. 2(b) we show the

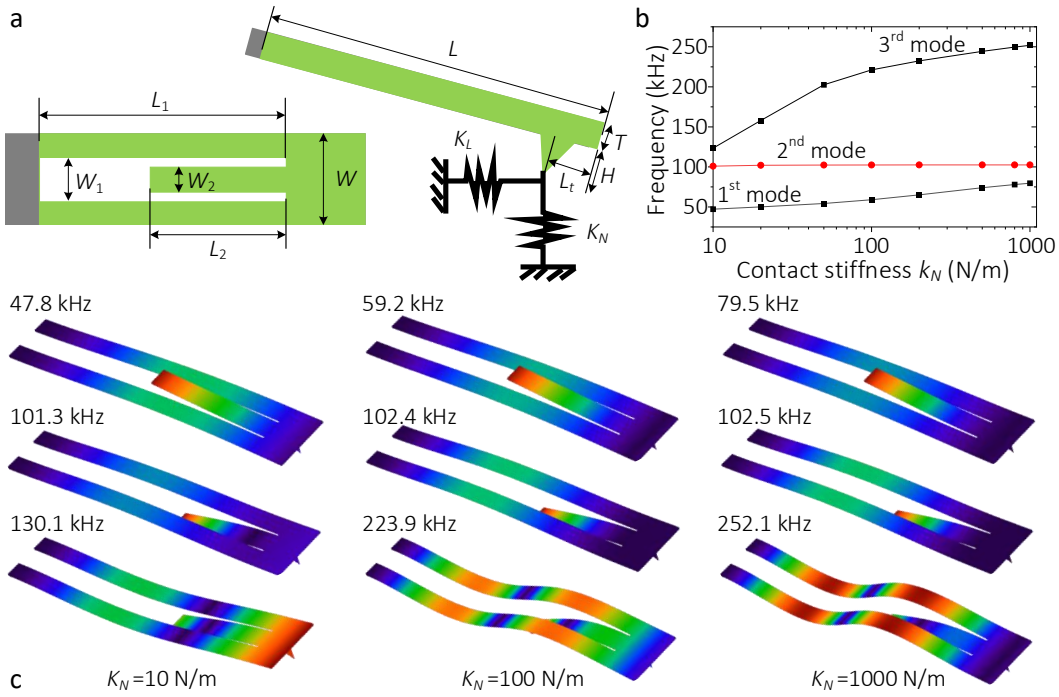

FIG. 2. (a) Schematic diagram of the inner-paddled cantilever model with tip-sample interaction represented by elastic springs; (b) The resonance frequencies calculated by FEA modal analyses of the first three flexural modes of an inner-paddled cantilever with parameters of $L = 450$ μm, $W = 50$ μm, $T = 2$ μm, $L_1 = 410$ μm, $W_1 = 20$ μm, $L_2 = 160$ μm and $W_2 = 16$ μm; (c) FEA-simulated mode shapes and their corresponding frequencies of the first three flexural modes of the inner-paddled cantilever for respective normal contact stiffnesses of 10, 100 and 1000 N/m.

calculated resonance frequencies of the first three flexural eigenmodes of a cantilever with $L_1 = 410$ μm, $W_2 = 16$ μm, $L_2 = 160$ μm, as functions of the normal contact stiffness. The simulated mode shapes of such a cantilever's first three flexural eigenmodes are accompanied in Fig. 2(c) for typical normal contact stiffnesses of respectively 10, 100 and 1000 N/m. It can be seen that the first and the third eigenmodes which correspond to the first two flexural eigenmodes of the base cantilever shift gradually to significantly higher frequencies by increasing the contact stiffness. This is expected from the resonance model of a surface-coupled cantilever beam [7, 8]. In addition, a second eigenmode can be seen to have a quite stable resonance frequency around 102 kHz, which is confirmed to correspond to the first flexural eigenmode of the inner cantilever. The mode shape of this eigenmode is seen to vary little compared to the other two eigenmodes by varying the contact stiffness (see Fig. 2(c)). A frequency change of only approx. 1.2 kHz is observed for this eigenmode within the contact stiffness range over 10∼1000 N/m.

Finally, the designed cantilevers that meets our target are fabricated. Here, we fabricate cantilevers with the same parameters as above (Fig. 2(b)). Although the fabrication can be done by etching with FIB based machining [17–20], here we carry out batch production based on a micromachining process as illustrated in Fig. 3. The fabrication starts on a 300 μm thick ⟨100⟩-oriented SOI (silicon on insulator) wafer which has a 15 μm thick top silicon layer and a 1 μm thick buried oxide layer (Fig. 3(a)). For the first step, the AFM tips are patterned by using E-beam lithography (6300FS, JEOL) and following anisotropic dry etching with SF_6 and O_2 at cryogenic temperature with a deep silicon etching system (Estrelas100, Oxford Instruments) (Fig. 3(b)). Then the inner-paddled cantilevers are patterned with maskless lithography (DWL 66+, Heidelberg Instruments) and following anisotropic dry etching with SF_6 and C_4F_8 (Figs. 3(c) and 3(d)). A 300 nm thick SiO_2 layer is then grown as shown in Fig. 3(e) by dry oxidation at 1000 °C for 4 hours in order to sharp the tips after etching the oxidation layer in later process. In addition, a thick layer of photoresist (PR) is coated as shown in Fig. 3(f) to protect the tip in the following process of fabricating the cantilevers by anisotropic deep dry etching of the wafer backside in a high inductive coupled plasma reactor (ICP380, Oxford Instruments) (Fig. 3(g)). Here, the buried oxide layer is used as the stop-etching layer and the photoresist layer is removed by acetone afterwards. The top and backside oxide layers are then etched as shown in Fig. 3(h) with a hydrofluoric acid (HF) vapor phase etching system, which is a convenient technique to release fragile, suspended structures. Finally, a 30 nm thick Aluminum (Al) layer is deposited by using an Ebeam evaporator system (Lab 18, Kurt J. Lesker Company) on the backside of the cantilever which serves as the reflecting layer

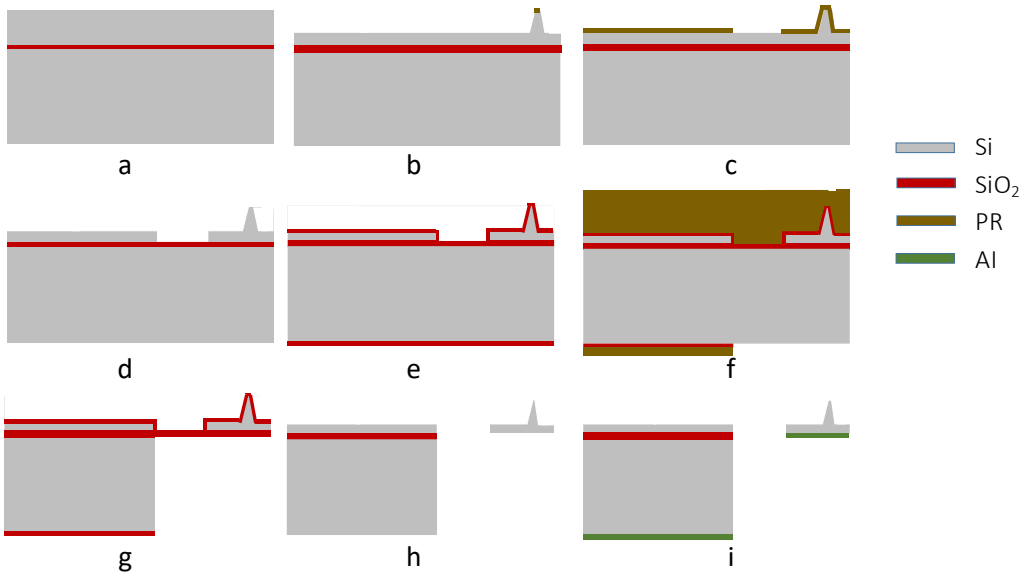

FIG. 3. Diagrams of the fabrication process of inner-paddled cantilevers.

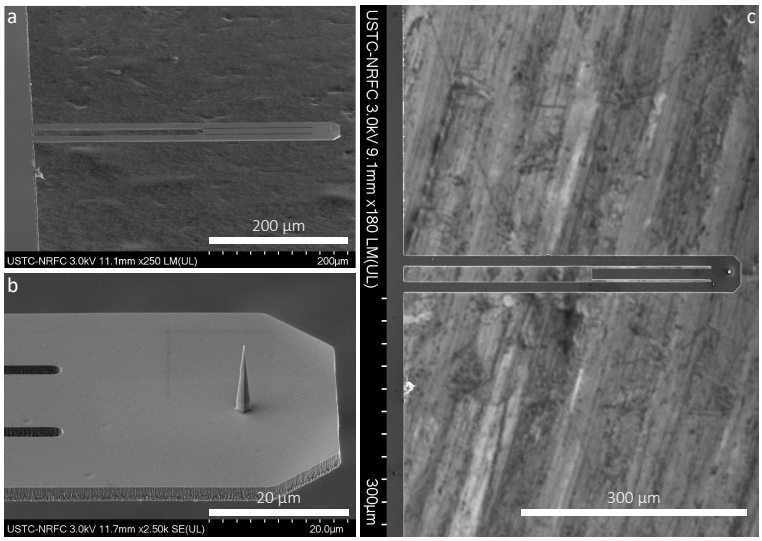

FIG. 4. Scanning electron microscope images of (a) a fabricated inner-paddled cantilever and (b) its tip end in sideviews, as well as (c) another cantilever in top view.

for optical detection in AFM (Fig. 3(i)). Such resulting cantilevers are shown in Fig. 4 by their scanning electron microscope (SEM) images (SU8220, Hitachi, Japan).

3. RESULTS AND DISCUSSION

3.1. Verification Measurements.

To verify that the proposed inner-paddled cantilever indeed provides an eigenmode whose resonance frequency is not sensitive to the contact stiffness changes, we first carried out spectroscopy measurements of the cantilever both in free air and while the tip is brought into contact with a sample surface with different tip loads. A polystyrene (PS) sample with a nominal Young's modulus of 2 GPa, as provided by the manufacturer Bruker, is used for the measurements. The measurements are performed on a commercial AFM (Dimension Icon, Bruker, CA) with excitations provided by the shake-piezo in the cantilever holder with the same amplitude of 100 mV. The free resonance (FR) spectrum of the cantilever, as shown in Fig. 5(a), illustrates resonances at around 14 (FR^1), 90 (FR^2), and 343 kHz (FR^3) which correspond to the free resonances of the base cantilever. Additionally, a resonance at around 141 kHz (FR^{inner}) can also be seen which is induced by the inner cantilever. When the tip is brought into contact with the PS sample, shifts

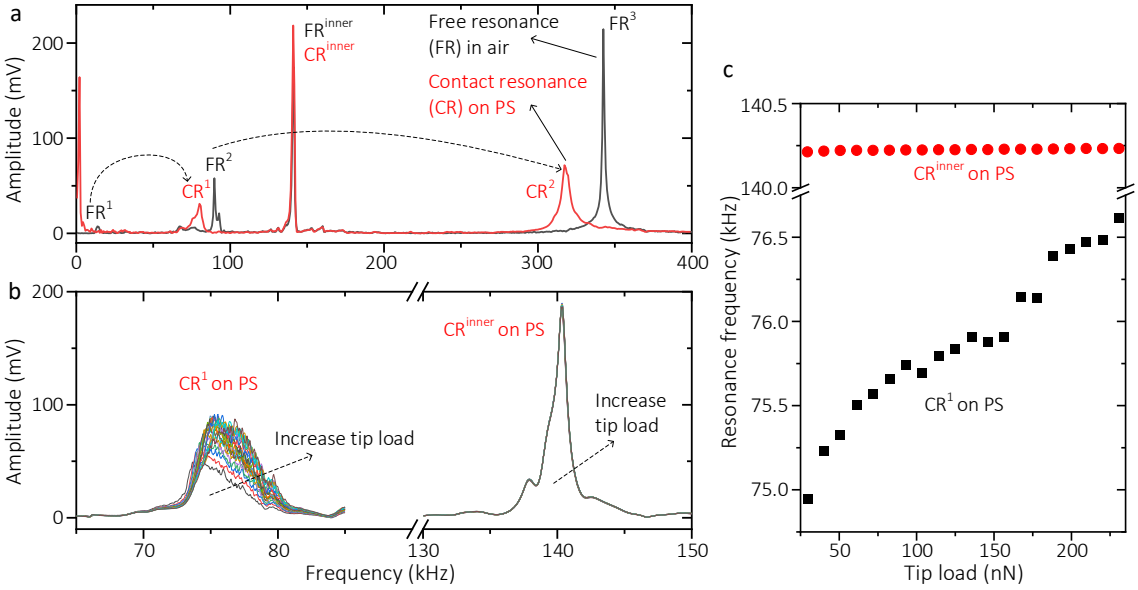

FIG. 5. (a) Resonance spectra of the inner-paddled cantilever measured respectively in free air and while its tip contacting a PS sample; (b) The resonance spectra and (c) the resonance frequencies of the first contact resonance of the base cantilever and of the inner cantilever measured at various tip loads on the PS sample.

of the first two resonances (FR^1, FR^2) of the base cantilever to higher contact resonances (CR) at respectively around 80 (CR^1) and 317 kHz (CR^2) can be clearly observed. However, the contact resonance corresponding to the inner cantilever (CR^{inner}) can be observed to coincide with its free resonance. Furthermore, by changing the applied tip loads which induces various contact stiffnesses, we can observe from the spectra and the resonance frequencies shown in Figs. 5(b) and 5(c) that the resonance induced by the inner cantilever (CR^{inner}) again keeps stable. However, the first contact resonance of the base cantilever shifts to higher frequencies with increasing the tip loads, which agrees with our analyses in Fig. 2(b). This indicates that the inner-paddled cantilever indeed provides a new eigenmode whose resonance keeps stable for varying contact stiffness.

It should be mentioned that the fabricated cantilever reported here demonstrates a resonance frequency of approx. 141 kHz, showing a deviation from the simulated one of around 102 kHz, see Fig. 2(b). We suggest that this is largely due to the deviation of the cantilever thickness from the assumed one of 2 μm, which is difficult to be precisely controlled in fabrication and plays the major role in affecting the cantilever's resonances. By adopting $L = 446$ μm, $W = 49$ μm, $L_1 = 407$ μm, $W_1 = 21$ μm, $L_2 = 158$ μm and $W_2 = 15$ μm for the cantilever, as measured by SEM imaging (see Fig. 4(c)), our FEA simulation indicates that the measured resonance frequency corresponds to a cantilever thickness of approx. 2.7 μm, and such a cantilever still meets our design target as also confirmed by the experiments here.

Next, we investigate how the amplitude of the new eigenmode induced by the inner cantilever responds to contact stiffness changes. To do so, contact resonance spectra corresponding to the inner cantilever are measured for different tip loads. Both the PS sample and a stiffer sample of fused silica with a nominal Young's modulus of 72.9 GPa, also provided by the manufacturer Bruker, are used for the measurements. It can be seen again from the spectra on both samples shown in Fig. 6(a) that the resonance induced by the inner cantilever shows almost unchanged frequency on both the fused silica and PS samples. In fact, measurements on both samples under various tip loads show that the resonance frequency deviates as little as 0.011 kHz. Although the new eigenmode induced by the inner cantilever, which is of our concern, isn't sensitive in its frequency to contact stiffness changes, its amplitude does change sensitively. This can be seen from the higher peak amplitude on the stiffer fused silica sample than on the PS sample as shown in Fig. 6(a). To more clearly reveal the amplitude response of the eigenmode induced by the inner cantilever to contact stiffness variations, we measure its peak amplitudes on both the fused silica and the PS sample for various tip loads under the same excitation amplitude. The results are shown in Fig. 6(b). It can be seen that for all the tip loads, the cantilever indeed shows larger resonance amplitudes on the stiffer fused silica sample than on the PS sample. In addition, with increasing the tip loads which means an increase of the contact stiffness [7], the resonance amplitude increases monotonously for both samples. This indicates that the proposed cantilever can be employed to distinguish samples with different moduli or to map the stiffness distribution of a sample surface at least semi-quantitatively by simply measuring its resonance amplitude.

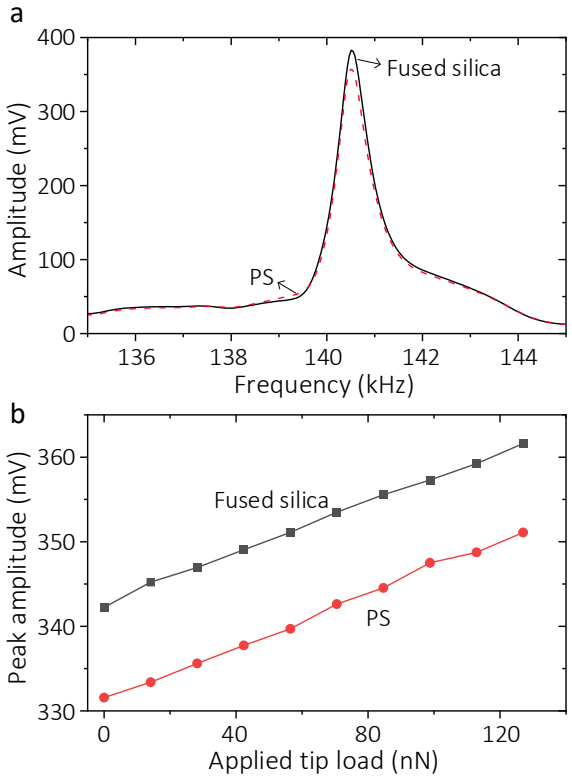

FIG. 6. (a) The resonance spectra near the eigenmode induced by the inner cantilever recorded while the tip is respectively in contact with a fused silica and a PS sample; (b) The peak amplitudes of the resonance induced by the inner cantilever recorded respectively on the fused silica and PS samples under various applied tip loads (not including adhesion).

It should be mentioned here that quantification of the applied tip loads in AFM requires the knowledge of the sensitivity of the optical lever detection scheme, that is the so-called inverse optical lever sensitivity (*invOLS*) [21], as well as the spring constant of the cantilever k_C. The *invOLS* parameter can be calibrated by recording a force-distance curve on a stiff sample. The inverse slope of the contact part of the force curve then yields the *invOLS*. Here, the *invOLS* is calibrated to be 243.3 nm/V. The spring constant k_C of a normal rectangular cantilever can be calibrated by using for example the thermal noise method [22]. However, this is not applicable for the proposed inner-paddled cantilever here which alters the shape and mass of the cantilever. Therefore, the spring constant k_C of the inner-paddled cantilever is estimated by calculating the deflection of the cantilever for a known load applied at the tip by using FEA. This yields a k_C of approx. 0.29 N/m, which is approx. 60% of the original base cantilever without the inner cantilever. Then the applied tip loads are quantified by multiplying the applied loads in voltage (setpoints) with *invOLS* and k_C.

3.2. Rapid Mechanical Mapping.

Here we demonstrate the capability of the proposed inner-paddled cantilever probe for rapid mechanical mapping. The experiments are carried out on a sample containing MoS_2 nanosheets that are suspended over well-defined circular holes on a silicon oxide wafer which has an oxidation thickness of 300 nm (XFNANO, Nanjing, China). The optical image of the MoS_2 sheet on which our measurements are performed is shown in Fig. 7(a). The thickness of the MoS_2 sheet is determined to be approx. 46 nm by measuring with the AFM at its edge. It covers circular holes with depths of around 2 μm and different radii of approx. 5, 4, 3, and 1 μm. As illustrated in Fig. 7(b), the suspend of the MoS_2 sheet over the holes creates edge-clamped circular plate structures whose stiffness k_S decrease gradually from their edges to the centers which can be described by [23]

$$k_S = \frac{16\pi D r_0^2}{(r_0^2 - r^2)^2}, \tag{1}$$

where $D = E_s t^3/(12(1-\nu_s^2))$ is the flexural rigidity of the plate, E_s is its Young's modulus and ν_s is its Poisson's ratio, t is its thickness, r_0 is its radius, and $r \leq r_0$ is the distance from its center.

In Figs. 7(c) and 7(d), we show the simultaneously obtained topography and amplitude images of an area at the edge of the MoS_2 sheet by using the proposed inner-paddled cantilever. The excitation frequency is set as 140.4 kHz which is at the resonance of the inner cantilever (see Fig. 6(a)), and an excitation amplitude of 100 mV is used. It can be seen that the covered holes are barely distinguishable from the topography, however they are clearly revealed by the amplitude image due to their stiffness differences from the supported region. In addition, the amplitude can be observed to decrease gradually from the supported region to the centers of the covered holes. This can be more clearly seen from the amplitude profiles shown in Fig. 7(e) which are extracted across the centers of four structures with different sizes as indicated in Fig. 7(d). Furthermore, smaller amplitudes are seen at the centers of structures over larger holes. Such observations meet the expectations of Eq. (1) that the stiffness of an edge-clamped circular plate structure decreases from its edge to its center, and that a larger such structure has a smaller stiffness at its center. This thus demonstrates that the proposed inner-paddled cantilever indeed can be used for at least semi-quantitative mapping of sample stiffness with rapid amplitude imaging.

To compare with the amplitude imaging by conventional contact resonance AFM, we show in Fig. 8 the contact-resonance AFM amplitude images of an area on the same sample as in Fig. 7 which contains two buried hole structures. The measurements are done by working at the first contact-resonance of the inner-paddled cantilever. Different working frequencies around the resonance ranging over 60 kHz to 80 kHz are employed.

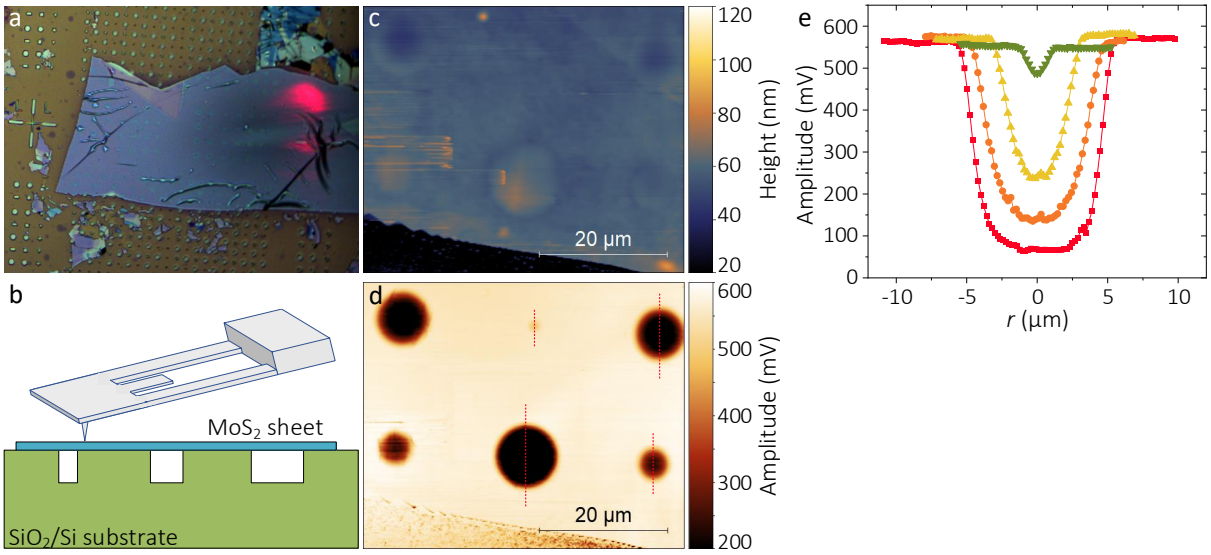

FIG. 7. (a) Optical image of a MoS_2 sheet with a thickness of approx. 46 nm overlaying on top of a SiO_2/Si substrate with arrays of circular holes; (b) Schematic diagram showing the inner-paddled cantilever scanning over the MoS_2 sheet that is suspended over holes on the SiO_2/Si substrate; (c) and (d) Topography and amplitude images of an area at the edge of the MoS_2 sheet that are simultaneously obtained by using the inner-paddled cantilever with a working frequency 140.4 kHz set at the resonance of the inner cantilever; (e) Amplitude profiles extracted across the centers of four suspended MoS_2 regions over holes with different sizes as indicated by dotted lines in (d).

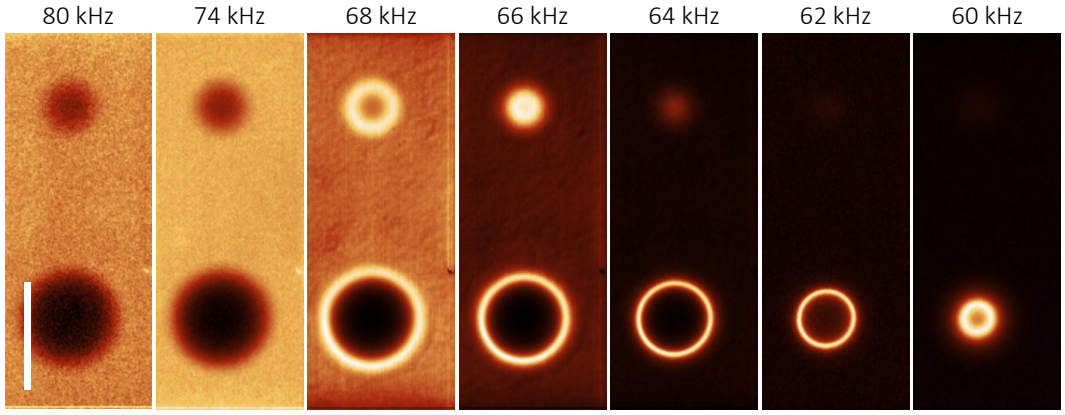

FIG. 8. Contact-resonance AFM amplitude images using the first contact resonance of the inner-paddled cantilever of an area containing two holes on the SiO_2/Si substrate covered by the MoS_2 sheet as in Fig. 7. Different working frequencies as indicated are employed. Scalebar: 10 μm.

Since the first contact-resonance of the cantilever shifts for different contact stiffnesses (see Fig. 5(a)), the contrasts of the subsurface features are therefore observed to change for different working frequencies. It is therefore difficult to infer which structure or which part of the structure is stiffer from such amplitude images of the conventional contact-resonance AFM. To quantitively characterize the structure stiffness, time-consuming contact-resonance AFM spectroscopy measurements are required [24]. A detailed explanation of the observed contrasts as in Fig. 8 can be found in Ref. [24].

Next, we explore how the amplitude imaging with the inner-paddled cantilever responds to contact stiffness variations. In Fig. 9(a), we show again the amplitude image around the MoS_2 structure suspended over one of the largest hole on the SiO_2/Si substrate, as well as the profile across its center. The gradual decrease of the amplitude from the supported region to the structure center indicates a similar trend of the contact stiffness sensed by the tip. While the AFM is indenting on the suspended structure, the contact stiffness k_N between the tip-sample can be regarded as a series connection of the stiffness k_S of the suspended plate structure and of the stiffness k_M due to local material deformation [24], that is $k_N = 1/(1/k_M + 1/k_S)$, as illustrated in the inset of Fig. 9(a). Since k_s of an edge-clamped circular plate

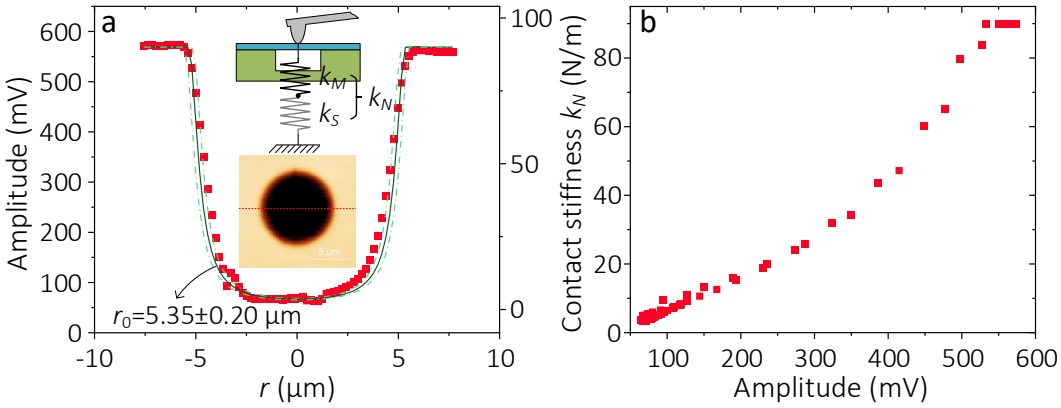

FIG. 9. (a) The amplitude image (inset) of a suspended MoS_2 structure over a hole on the SiO_2/Si substrate that has the largest radius, and a profile extracted across its center (data points). A schematic model (inset) of the contact stiffness sensed by the tip while contacting above the suspended MoS_2 sheet is also shown, as well as the calculated contact stiffness (solid line) across the structure considering a structure radius of 5.35 μm with the strip range representing errors for a structure radius deviation of ± 0.20 μm; (b) Contact stiffness as a function of the measured amplitude.

structure decreases from its edge to the center, see Eq. 1, and k_M keeps constant for same experimental setups, a gradual decrease of k_N is indeed expected from the supported region to the structure's center.

More quantitatively, by applying contact-resonance spectroscopy measurement on the supported region, we obtain contact resonance frequency of approx. 73.0 kHz for the first eigenmode of the cantilever. This results in a contact stiffness of $k_N = k_M \approx 90$ N/m by using our FEA model on the supported region where k_S becomes infinite. Then, by further calculating k_S using Eq. (1), we obtain the contact stiffness sensed by the tip across the center of the suspended structure. Here, a Young's modulus of $E_s = 238$ GPa and a Poisson's ratio of $\nu_s = 0.27$ is adopted for the MoS_2 sample [25]. The radius of the covered hole is considered to be approx. $r_0 = 5.35$ μm, as measured for a similar uncovered one on the bare substrate, with an error of $\pm$ 0.20 μm being considered for fabrication and measurement deviations. The resulting contact stiffness across the structure center is then shown in Fig. 9(a). By overlaying it with the measured amplitude profile, it can be seen that the amplitude imaging with the inner-paddled cantilever indeed reveals contact stiffness variations of the structure quite well.

Furthermore, from the amplitude measurements and the contact stiffness estimations in Fig. 9(a), we relate the inner-paddled cantilever' amplitude to the tip-sample contact stiffness as shown in Fig. 9(b). A monotonous increase of the resonance amplitude can be observed with increasing the contact stiffness, which agrees with our discussion before. Such a relation then leads to the possibility of using it for contact stiffness calibration for measurements on other samples.

Finally, let us give a brief discussion on the lateral resolution of the mechanical imaging using the inner-paddled cantilever. As same as in other AFM imaging methods based on the contact mode, for example contact-resonance AFM, the lateral resolution of imaging with the inner-paddled cantilever is determined by the tip-sample contact radius and is typically below 10 nm [9]. For instance, considering a tip radius R of approx. 90 nm as measured for one of our cantilever by SEM, a typical tip load of F_N=100 nN results in a lateral resolution that is comparable to the contact radius of $a_c = (3F_N R/4E^*)^{1/3} \approx 4.0$ nm according to the Hertzian contact model [7]. Here, $E^* = 1/((1-\nu_t^2)/E_t + (1-\nu_s^2)/E_s)$, we use E_t=169 GPa, ν_s=0.27 for the silicon tip, and adopt E_s and ν_s of MoS_2 as above.

4. CONCLUSIONS

In summary, we have proposed an inner-paddled AFM cantilever design for semi-quantitative mechanical mapping with fast amplitude imaging. The proposed cantilever contains a secondary small cantilever that is integrated inside a normal rectangular cantilever. The cantilever was designed to provide a resonance mode whose frequency keeps relatively stable within a broad range of contact stiffness, whereas its amplitude corresponds monotonically to the changes of the tip-sample contact stiffness. The capability of the proposed inner-paddled cantilever for rapid semi-quantitative stiffness mapping by amplitude imaging was demonstrated. The possibility of quantitative contact stiffness calibration from the amplitude measurement was also discussed. The proposed inner-paddled AFM cantilever avoids the problem of time-consuming spectroscopy measurement by frequency sweep for quantitative mechanical characterization in conventional contact-resonance AFM. It is hoped to serve as an alternative method for fast semi-quantitative mechanical mapping, with the possibility of further quantitative calibration.

ACKNOWLEDGMENTS

We acknowledge the support from National Natural Science Foundation of China (No. 52005476), Hefei Municipal Natural Science Foundation (No. 2021014) and Chinese Academy of Sciences Instrument and Equipment Function Development Technology Innovation Project (No. PECU2019001). This work was partially carried out at the USTC Center for Micro and Nanoscale Research and Fabrication.

DATA AVAILABILITY

Data supporting the findings of this study are available from the corresponding author upon reasonable request.

CONFLICT OF INTEREST

The authors declare no competing financial interest.

REFERENCES

[1] M. F. Pantano, H. D. Espinosa, and L. Pagnotta, Mechanical characterization of materials at small length scales. *Journal of Mechanical Science and technology*, **26**, 545-561 (2012).

[2] G. Binnig, C. F. Quate, and C. Gerber, Atomic force microscope. *Physical Review Letters*, **56**(9), 930 (1986).

[3] R. Garcia, Nanomechanical mapping of soft materials with the atomic force microscope: methods, theory and applications. *Chemical Society Reviews*, **49**(16), 5850-5884 (2020).

[4] B. Cappella and G. Dietler, Force-distance curves by atomic force microscopy. *Surface Science Reports*, **34**(1-3), 1-104 (1999).

[5] Y. F. Dufrêne, D. Martínez-Martín, I. Medalsy, D. Alsteens, and D. J. Müller, Multiparametric imaging of biological systems by force-distance curve–based AFM. *Nature Methods*, **10**(9), 847-854 (2013).

[6] R. Garcia and E. T. Herruzo, The emergence of multifrequency force microscopy. *Nature Nanotechnology*, **7**(4), 217-226 (2012).

[7] U. Rabe, M. Kopycinska-Müller, and S. Hirsekorn, in *Acoustic Scanning Probe Microscopy*, edited by F. Marinello, D. Passeri, and E. Savio (Springer, Berlin, 2013), pp. 123–153.

[8] J. P. Killgore and F. W. DelRio, Contact resonance force microscopy for viscoelastic property measurements: from fundamentals to state-of-the-art applications. *Macromolecules*, **51**(18), 6977-6996 (2018).

[9] C. Ma and W. Arnold, Nanoscale ultrasonic subsurface imaging with atomic force microscopy. *Journal of Applied Physics*, **128**(18), 180901 (2020).

[10] C. Ma, Y. Chen, and T. Wang, Image contrast reversals in contact resonance atomic force microscopy. *AIP Advances*, **5**(2), 027116 (2015).

[11] B. J. Rodriguez, C. Callahan, S. V. Kalinin, and R. Proksch, Dual-frequency resonance-tracking atomic force microscopy. *Nanotechnology*, **18**(47), 475504 (2007).

[12] S. Jesse, S. V. Kalinin, R. Proksch, A. P. Baddorf, and B. J. Rodriguez, The band excitation method in scanning probe microscopy for rapid mapping of energy dissipation on the nanoscale. *Nanotechnology*, **18**(43), 435503 (2007).

[13] S. Bradler, A. Schirmeisen, and B. Roling, Piezoresponse force and electrochemical strain microscopy in dual AC resonance tracking mode: analysis of tracking errors. *Journal of Applied Physics*, **123**(3), 035106 (2018).

[14] R. Potekin, S. Dharmasena, H. Keum, X. Jiang, J. Lee, S. Kim, L. A. Bergman, A. F. Vakakis, and H. Cho, Multifrequency Atomic Force Microscopy based on enhanced internal resonance of an inner-paddled cantilever. *Sensors and Actuators A: Physical*, **273**, 206-220 (2018).

[15] S. M. Dharmasena, Z. Yang, S. Kim, L. A. Bergman, A. F. Vakakis, and H. Cho, Ultimate decoupling between surface topography and material functionality in atomic force microscopy using an inner-paddled cantilever. *ACS Nano*, **12**(6), 5559-5569 (2018).

[16] P. E. Mazeran and J. L. Loubet, Normal and lateral modulation with a scanning force microscope, an analysis: Implication in quantitative elastic and friction imaging. *Tribology Letters*, **7**, 199-212 (1999).

[17] Y. Hou, C. Ma, W. Wang and Y. Chen, Binary coded cantilevers for enhancing multi-harmonic atomic force microscopy. *Sensors and Actuators A: Physical*, **300**, 111668 (2019).

[18] J. Cai, Q. Xia, Y. Luo, L. Zhang, and M. Y. Wang, A variable-width harmonic probe for multifrequency atomic force microscopy. *Applied Physics Letters*, **106**(7), 071901 (2015).

[19] D. T. Edwards, J. K. Faulk, A. W. Sanders, M. S. Bull, R. Walder, M. A. LeBlanc, M. C. Sousa, and T. T. Perkins, Optimizing 1-μs-resolution single-molecule force spectroscopy on a commercial atomic force microscope. *Nano Letters*, **15**(10), 7091-7098 (2015).

[20] B. Zhu, S. Zimmermann, X. Zhang, and S. Fatikow, A systematic method for developing harmonic cantilevers for atomic force microscopy. *Journal of Mechanical Design*, **139**(1), 012303 (2017).

[21] M. J. Higgins, R. Proksch, J. E. Sader, M. Polcik, S. Mc Endoo, J. P. Cleveland, and S. P. Jarvis, Noninvasive determination of optical lever sensitivity in atomic force microscopy. *Review of Scientific Instruments*, **77**(1), 013701 (2006).

[22] J. L. Hutter, and J. Bechhoefer, Calibration of atomic-force microscope tips. *Review of Scientific Instruments*, **64**(7), 1868-1873 (1993).

[23] R. Szilard, *Theories and Applications of Plate Analysis: Classical Numerical and Engineering Methods* (John Wiley & Sons, Inc., Hoboken, NJ, 2004), pp. 161–165.

[24] C. Ma, W. Wang, Y. Chen, W. Arnold, and J. Chu, Depth-sensing using AFM contact-resonance imaging and spectroscopy at the nanoscale. *Journal of Applied*

Physics, **126**(12), 124302 (2019).

[25] J. L. Feldman, Elastic constants of 2H-MoS2 and 2H-NbSe2 extracted from measured dispersion curves and linear compressibilities. *Journal of Physics and Chemistry of Solids*, **37**(12), 1141-1144 (1976).